X-ray detection by superconducting tunnel junctions via phonon propagation in the substrate

A. Poelaert, C. Erd, A. Peacock, N. Rando, and P. Verhoeve
Astrophysics Division, Space Science Department, European Space Agency, ESTEC, Noordwijk, The Netherlands

A. G. Kozorezov and J. K. Wigmore
School of Physics and Chemistry, Lancaster University, Lancaster, United Kingdom

(Received 14 November 1995; accepted for publication 16 January 1996)

The x-ray performance of Nb-Al-AlO_x-Al-Nb superconducting tunnel junctions deposited on sapphire has been studied for phonon mediated detection of x rays absorbed in the substrate in the energy range 750 to 6000 eV. Two separate channels of phonon propagation can be identified. One produces a discrete signal peak, due to high frequency phonons originating from the x-ray absorption sites in a shallow layer below the junction. The other contributes to a monotonic signal tail, due to low frequency phonons, reaching the junction after diffusive or multiple scattering at surfaces. © *1996 American Institute of Physics.* [S0021-8979(96)01709-5]

I. INTRODUCTION

Superconducting tunnel junctions (STJ) have provided x-ray detectors with good energy resolution ($<1\%$ for 6 keV incident photons directly absorbed in the superconducting thin films comprising the STJ[1–3]).

Devices which have achieved these results have very poor quantum efficiencies: their film thicknesses are too small to stop these energetic x-ray photons, and as a result most of the 6 keV incident photons are absorbed in the substrate.

A simple increase in the thickness of the STJ is not a viable solution, since this would decrease the tunneling probability of the quasiparticles (charge carriers created by the breaking of Cooper pairs). Such a decrease would lead to a reduction in the measured signal and a resultant degradation in the energy resolution. A number of groups have examined the problem of absorption efficiency by the use of alternative higher Z superconductors such as tantalum (Z=73) rather than Nb (Z=41) or Al (Z=13).[2] An alternative approach is to detect the x-ray events which are not directly absorbed in the thin superconductive film, but in the substrate, by measuring the energy reaching the junction via phonon propagation from the substrate. A sufficient portion of the energy of these events can be down-converted into phonons which cross the substrate–junction interface and break Cooper pairs in the superconductive electrode of the STJ.

Several authors have argued that this detection can take place in an efficient way, even when absorption takes place very deep in the substrate, because of phonon focusing due to the elastic anisotropy of the crystal used as the substrate.[4–6] The anisotropy focusses a significant portion of the phonon flux, which hence propagates along preferential directions called *caustics*. As a consequence, a much larger fraction of the phonon flux, arising from a photoabsorption site in the substrate, may reach the STJ than would be expected purely from a consideration of the solid angle subtended by the STJ, as long as the crystallographic alignment of the substrate is correct. Then the charge output of the STJ will be proportional to this flux, which is proportional to the energy of the incident x-ray photon.

The aim of this article is to evaluate the feasibility and characteristics of x-ray detection via phonon propagation in the substrate. We shall see that the substrate events delivering the largest fraction of their energy to the STJ are clearly separated from other events (Secs. II and III). The detection efficiency, response and resolution of this process will be described in Sec. IV and its detailed mechanism discussed in Sec. V. Special attention is accorded to the region of the substrate where such events occur. Various x-ray energies in the range 750 eV to 6000 eV and two junction sizes were used.

II. EXPERIMENTAL OBSERVATION OF SUBSTRATE EVENTS

A. Experimental configuration

All measurements presented here were based on a substrate made of single crystal sapphire. Sapphire has a space group R3c, with a trigonal cell ($\alpha = 85°43'$, $a = 6.9$ Å). A sample 0.5 mm thick with an impurity level of 23 ppm has been grown to have an orientation of $[\bar{1}102]$ (i.e. the *R*-plane orientation) for the plane of the substrate-junction interface. The ballistic phonon flux pattern in such a crystal has been measured and calculated by Every *et al.*[7]

On the substrate a set of 8 junctions was deposited. Their base electrodes were layers of 110 nm of epitaxial Nb, on which a layer of 5 nm Al was deposited. The barrier was produced through the oxidation of part of this Al layer and had a resistivity of $\sim 2.5\times10^{-6}\,\Omega\,\mathrm{cm}^2$. The top electrode consisted of another 5 nm thick Al layer and 210 nm of polycrystalline Nb. Measurements were carried out with two junctions of sizes $20\times20\ \mu\mathrm{m}^2$ and $50\times50\ \mu\mathrm{m}^2$.

This system was placed in a vacuum environment and clamped to a cold finger, cooled via a pumped ^{4}He cryostat. A magnetic field was applied, by a superconducting magnet, in order to suppress the dc Josephson current.

The current pulses from the STJ were fed into a charge sensitive preamplifier and a shaping stage, operating at room

 0021-8979/96/79(9)/7362/8/$10.00

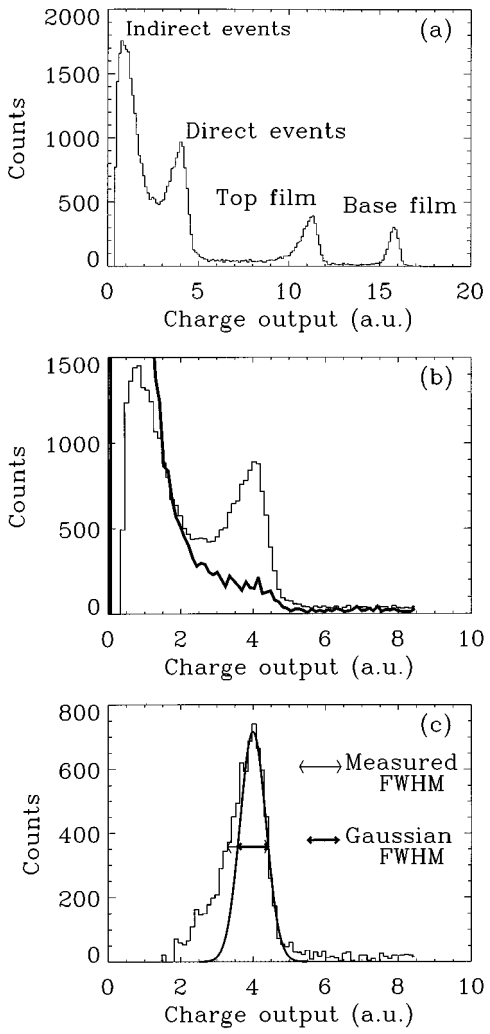

FIG. 1. (a) Spectrum acquired by a $20\times20\ \mu m^2$ device with an external beam of photons at 1600 eV; the various components from the external source are detailed. (b) Zoom in of Fig. 1(a) (thin line); fit of the indirect events contribution on this spectrum (thick line). (c) Result of the subtraction of the indirect events and Gaussian fit of the right edge of the remaining events; definition of measured and Gaussian FWHM.

temperature, and optically coupled to a PC. During all measurements, a test pulser was connected to the preamplifier, in order to monitor the electronic noise and linearity of the electronics.

B. Experiments performed

1. Observed spectrum

The substrate events spectrum was obtained as a function of energy from 750 eV to 6000 eV using monochromatized synchrotron radiation. A detailed description of the setup of this experiment can be found in Ref. 8. The temperature at the cold finger was about 1.38 K. An additional ^{55}Fe source was continuously illuminating the STJ to calibrate the gain of the detector.

Figure 1(a) shows a typical charge spectrum, corresponding to the irradiation of a $20\times20\ \mu m^2$ device by x-ray photons with an energy of 1600 eV. The contribution of the calibration source has already been removed from this spectrum. Several contributions are clearly seen: a) events with the highest charge output ($\sim$16 a.u.) correspond to the base Nb film response; b) the other isolated peak at $\sim$11 a.u. is the top Nb film contribution; the different numbers of counts in the top and base films are due to the different thicknesses of the electrodes; c) at the lowest charge outputs (below 5 a.u.), the substrate contributions can be seen.

The substrate events are in turn divided into two classes. The well-defined peak at higher charge outputs ($\sim$4 a.u.) presumably arises from those events occurring closest to the junction, say within a characteristic distance d_1 of the junction. We shall call this the *direct* peak; a full discussion of its origin will be given later. Finally, at the very lowest charge outputs, a broad non-resonant background can be seen. The appearance of a peak is an artifact created by the low charge cutoff of the electronics. It has been shown by Rando *et al.*[9] that the phonons generated by deep absorption events have a sufficient lifetime in sapphire to reach the junction, even after multiple scattering or reflections on the substrate boundaries. We believe that this *indirect* feature is due to diffusively propagating phonons. As we shall see, its magnitude does not depend on the lateral position of the x-ray beam relative to the STJ. In contrast, the direct feature is observed only when the STJ is directly illuminated.

2. Observation of indirect events

In order to have a better understanding of what are the direct and indirect events contributions, the spectral properties of the indirect events were established by two dedicated experiments. The substrate was illuminated by a collimated beam of Mn-K_α (5895 eV) and Mn-K_β (6490 eV) x-rays excited by the decay of ^{55}Fe. In the first experiment the x-ray source was placed on the junction side of the substrate (*front-illumination*), but some 2 mm away. For the second experiment, the substrate was illuminated from the opposite side (*back-illumination*). In both cases, the position of the cold finger was also varied in the plane of the junction-substrate interface, in order to evaluate any possible spatial fluctuation in the response. A similar scanning system has been described in Ref. 10. The temperature of the cold finger was set at 1.2 K and 1.38 K.

The charge spectra obtained from both measurements were identical to within 2% and could be scaled to correspond to the indirect feature of Fig. 1(a). No dependence on the position of the cold finger was found. This supports the identification of the lowest observed charge outputs as arising as a result of phonon multiple scattering and reflections on the substrate boundaries. Finally, no temperature dependence of the indirect peak was observed.

III. EXTRACTING THE DIRECT EVENTS

To extract the direct events from the data delivered by the experiment described in Sec. II B 1, the indirect events must be removed. This operation has been performed by scaling the spectrum obtained from the measurements described in Sec. II B 2. This scaling was based not only on the difference in energy of the incident x-rays (5895 eV for the

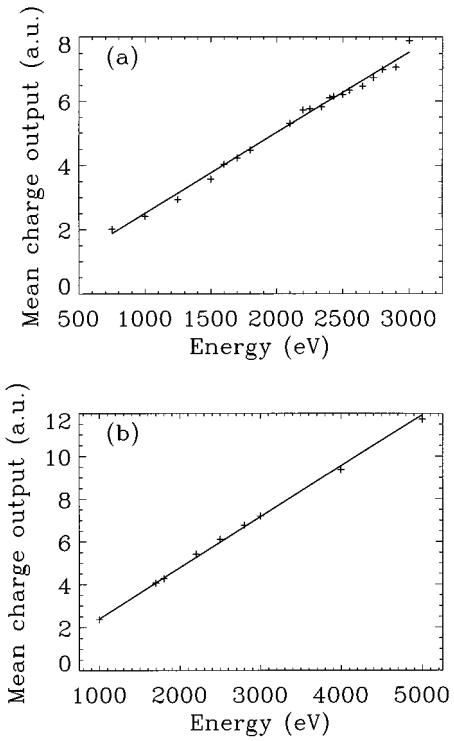

FIG. 2. Mean charge output of the direct events as a function of energy (a) for the 20×20 μm^2 device (b) for the 50×50 μm^2 device. The solid lines are linear fits of the data.

indirect events and between 750 eV and 6000 eV for the basis spectrum), but also on the observed non linearity of the STJ.[8]

Figures 1(b) and 1(c) illustrate the subtraction of indirect events from the initial spectrum of Fig. 1(a). The thin line in Fig. 1(b) is an enlargement of Fig. 1(a) in the substrate events region. The dashed line is an overplot of the scaled indirect events. The inconsistency at low charge values results from this scaling, which also incorrectly scales the constant event threshold. This scaled spectrum is subsequently subtracted, resulting in the residual direct events spectrum of Fig. 1(c). Similar results were obtained for energies in the range of 1000 to 5000 eV with the 50×50 μm^2 device and 1000 to 3000 eV with the 20×20 μm^2. The spectrum of the direct events can be described adequately by a Gaussian curve skewed at the lower charge values. Since the base film response at $\sim$16 a.u. is nearly perfectly Gaussian (see Ref. 8), it is reasonable to assume that the true direct events give rise to the Gaussian portion. The presence of the low charge tail can perhaps be explained by the detection of quasi-direct events, absorbed in the transitional region separating direct and indirect events.

IV. X-RAY PERFORMANCE OF THE DIRECT EVENTS

A. Charge output

The charge output Q_{out}, corresponding to the mean of the Gaussian in Fig. 1(c), is plotted as a function of energy in Fig. 2. This response is linear to less than 3% for the 50×50 μm^2 device and 5% for the 20×20 μm^2 device (in the energy range 1000 to 5000 eV and 750 to 3000 eV, respectively).

In the case of a 50×50 μm^2 device, Q_{out} is about 30% of the charge output from base film events. For the 20×20 μm^2 device, this figure is lowered to 25%.

The ratio of the substrate events charge output with the base film events charge output Q_b has an important physical interpretation. Once inside this electrode, a phonon has a lifetime of about 4.17 ps[11] against Cooper pair breaking in Nb, corresponding to a mean free path of $\sim$30 nm. Thus, in base films of 100 nm thick, all the phonons are converted into detectable quasiparticles before crossing the tunnel barrier into the top film. Hence, the ratio of the charge output for substrate events to the charge output for base film events directly relates the fraction of its energy that the substrate event has sent to the STJ.

B. Energy resolution

The energy resolution ΔE (FWHM=Full width at half maximum) of a STJ is a combination of the Fano limited resolution σ_F, the statistical fluctuations in the number of electrons that tunnel across the barrier σ_{tun}, the electronic noise contribution σ_e and the variations due to spatial inhomogeneities σ_s:

$$\Delta E = 2.355\sqrt{\sigma_F^2+\sigma_{\text{tun}}^2+\sigma_e^2+\sigma_s^2}. \tag{1}$$

For absorption events occurring within the substrate, the effects due to phonon propagation can be included in the spatial fluctuations.

If the quasiparticle self-recombination is neglected, σ_F^2 and σ_{tun}^2 are proportional to the energy E of the incident photon.[9,12] The base film contribution to these two variances is estimated at $\sim$12 eV (FWHM) at $E=6$ keV,[8] which is negligible compared to the contributions of the electronics and the spatial fluctuations.

The electronic noise can be calculated by observing the FWHM of the peak given by the pulser.

As for the spatial variations, the signal is the sum of a series of components, each being proportional to the energy E. Assuming that the proportionality factor is a function of the absorption site only—and not of E—the overall distribution has a sigma σ_s equal to the difference between 2 proportionality factors. This results in a variance $\sigma_s^2 \propto E^2$.

Figure 3 plots the energy resolution of the direct events ΔE_{-e}, after subtraction of the electronic noise. Two sets of data are presented: one is the FWHM as measured on the experimental peak, the other is the FWHM of the Gaussian fit. The difference between these two FWHM is indicated in Fig. 1(c).

The data points of the Gaussian FWHM could be fitted (solid lines in Fig. 3) by the function:

$$\Delta E_{-e} = \sqrt{a+bE+cE^2}. \tag{2}$$

b was fixed by the knowledge of σ_F and σ_{tun} at 0.024 eV^{-1},[8] a is a possible remaining offset and c provides a measure of the spatial contribution.

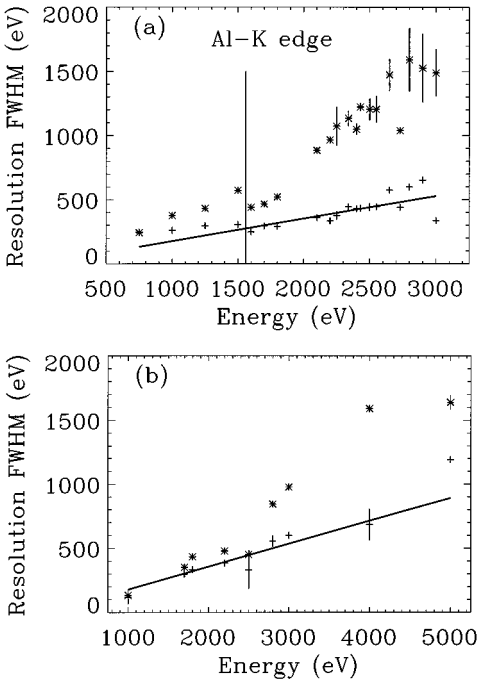

FIG. 3. Energy resolution as a function of the photon energy. The electronic contribution has been removed. The Gaussian FWHM are described by + (data points) and solid lines (fit). The measured FWHM are described by *. The fits are based on Eq. (2). (a) 20×20 μm^2 device. (b) 50×50 μm^2 device.

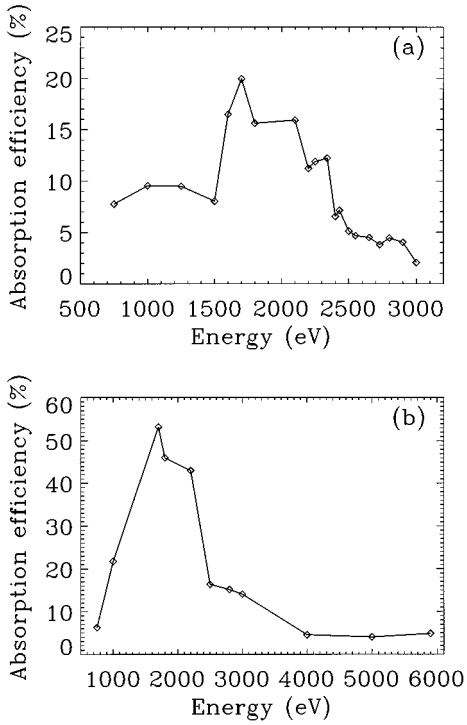

FIG. 4. Absorption efficiency for the direct events: (a) 20×20 μm^2 junction. (b) 50×50 μm^2 junction.

The experimental FWHM cannot be fitted by the same law. Indeed, it also includes the contribution due to quasi-direct events (see Secs. III and V C), which is expected to be directly related to the penetration depth for the photons in sapphire. As an example, it will be higher immediately below the Al-*K* edge (corresponding to a penetration depth of 2.9 μm) than immediately above it (penetration of 0.9 μm). The offset and the spatial contribution for the Gaussian FWHM are listed in Table I. In all cases, the offset is very small.

The measured FWHM is larger, especially for the 20×20 μm^2 device. Also in this case, the effect discussed above around the Al-*K* edge is clearly visible.

C. Absorption efficiency

The absorption efficiency for direct events can be defined as the ratio of the number of direct events N_d to the total number of detected events N_t. Figure 4 shows the observed efficiency for the two devices, which exceeds 50% in the case of the 50×50 μm^2 device.

TABLE I. Fitting parameters for the FWHM of the base film and substrate response.

Photoabsorption site	Device	Offset ($\sqrt{a}$) (eV)	Spatial contribution ($\sqrt{c}$) (eV/keV of E)
Base film	20×20 μm^2	⋯	15
(see Ref. 8)	50×50 μm^2	⋯	16
Substrate	20×20 μm^2	0.3	176
(Gaussian FWHM)	50×50 μm^2	0.4	178

According to the comments of Sec. II B 1, d_1 is an experimentally defined parameter; it is the distance from the STJ within which photon absorption events contribute to the direct peak. Instead of using N_d/N_t, we prefer N_d/N_b with N_b the number of events detected by the base film of the STJ, since N_b is easier to handle mathematically than N_t. If N_i is the number of photons incident on the Nb base film, then N_b is given by:

$$N_b = N_i[1-e^{-\mu_{\mathrm{Nb}}\rho_{\mathrm{Nb}}d_b}] \tag{3}$$

with μ_{Nb} the mass absorption coefficient in Nb, ρ_{Nb} the density of Nb and d_b the thickness of the base film.

Similarly, the number of events N_d absorbed in a sapphire substrate layer of thickness d_1 (direct events) is

$$N_d = N'[1-e^{-\mu_{\mathrm{sap}}\rho_{\mathrm{sap}}d_1}] \tag{4}$$

with

$$N' = N_i - N_b = N_i e^{-\mu_{\mathrm{Nb}}\rho_{\mathrm{Nb}}d_b}. \tag{5}$$

Here, the suffix sap is for ''sapphire.'' The ratio of direct events to base film events is then

$$\frac{N_d}{N_b} = e^{-\mu_{\mathrm{Nb}}\rho_{\mathrm{Nb}}d_b}\cdot\frac{1-e^{-\mu_{\mathrm{sap}}\rho_{\mathrm{sap}}d_1}}{1-e^{-\mu_{\mathrm{Nb}}\rho_{\mathrm{Nb}}d_b}}. \tag{6}$$

The only remaining unknown parameter in Eq. (6) is d_1. This parameter can be obtained from measurements of N_d and N_b as a function of incident photon energy. Integrating the Gaussian fit of Fig. 1(c) leads to N_d as a function of photon energy. N_b can be directly extracted from the data. The values of μ_{Nb} and μ_{sap} have been taken from Ref. 13. Figure 5

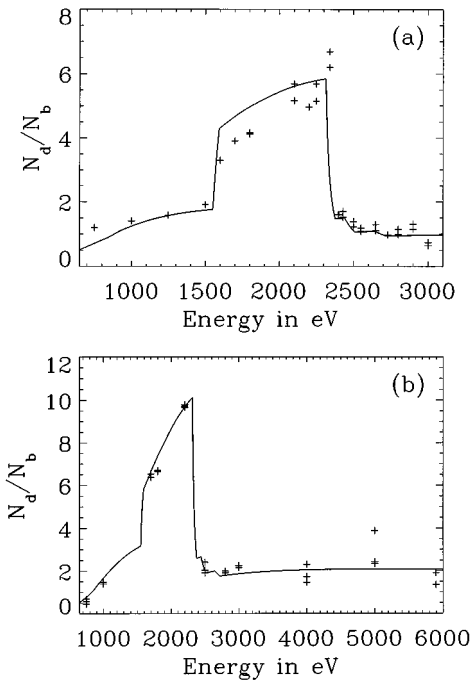

FIG. 5. N_d/N_b (a) for the 20×20 μm^2 device and (b) for the 50×50 μm^2 device, measured (+) and calculated with $d_1=1.041\pm0.083$ μm for the 20×20 μm^2 and 2.261 ± 0.182 for the 50×50 μm^2 (solid lines). These values of d_1 are derived from a least squares fit to the data.

shows the observed values of N_d/N_b as a function of energy, together with the best fit model. Best fit values of $d_1=1.041\pm0.083$ μm and 2.261 ± 0.182 μm for the 20×20 and 50×50 μm^2 respectively were derived. It is an important conclusion from these results that d_1 is independent of x-ray energy. That is, the thickness of the region giving rise to direct events does not depend on the thickness of the layer in which the x-rays are absorbed.

D. Summary of experimental observations

(1) Substrate signals can be resolved into two distinct contributions, direct and indirect, with very different characteristics.
(2) The indirect contribution is non-resonant and independent of the position of the absorption event relative to the STJ.
(3) The direct contribution is a well-defined peak, and is due to absorption events occurring within a distance d_1 of the STJ which does not depend on x-ray energy.
(4) The direct peak magnitude decreases relative to the indirect peak with increasing energy, while its linewidth scaled with x-ray energy.

V. DISCUSSION

A. Interpretation of the direct events

In this section we discuss the origin of the direct peak, and attempt to explain the experimental features summarized above.

We begin from the important observation that the volume of the region of the substrate from which the direct signal originates is independent of the energy of the absorbed x-ray. Thus, even when the x-ray energy, E, is increased so that the photons penetrate further into the substrate, still only those events occurring within a distance d_1 of the surface, and hence of the STJ, contribute to the direct peak. Consistent with this result is the additional observation that the direct peak decreases relative to the indirect feature with increasing E. The latter relates to events which occur deeper in the substrate so that the phonons produced suffer further scattering or decay before reaching the STJ. For the range of x-ray energies used in our experiments the absorption length lies between 0.5 and 30 μm, so that all x-rays are absorbed somewhere at least within the substrate. We find that the indirect magnitude scales with E, while as a fraction of this the direct peak, corresponding to the energy absorbed within a fixed thickness d_1, decreases with E.

In order to understand what may determine d_1, we must consider the process by which the incident x-ray photon is converted into phonons which may eventually reach the STJ. The absorbed photon directly excites a single primary electron which rapidly loses its energy by exciting a shower of secondaries along a track. Each secondary electron excites the cascade of optic phonons before finally subsiding back into a bound state. The frequencies of the optic phonons are in the broad range above 10 THz, and their lifetime against spontaneous decay into lower frequency acoustic phonons a few ps, corresponding to a mean free path of ~0.1 μm. The acoustic phonons produced typically have frequencies centered around half of that of their parents. Thus, each x-ray absorption site can be regarded as a point-like source of phonons around 5 THz. These phonons can subsequently undergo either further inelastic scattering, through anharmonic decay down to the next generation of 2–3 THz in frequency, or may be scattered elastically through Rayleigh scattering from isotopes, impurities or crystalline imperfections. We examine these alternatives in detail.

There are no direct measurements of anharmonic decay of acoustic phonons in sapphire at this frequency. However we may attempt to estimate the appropriate lifetime directly from experimental data at other frequencies and theoretical calculations for the spontaneous anharmonic decay in sapphire. The theoretical calculation by Berke[14] based on experimentally measured values of second and third order elastic constants in sapphire gives the following estimate for the average lifetime against anharmonic decay

$$\tau_a(\nu)\simeq\frac{1}{300}\left(\frac{\nu_D}{\nu}\right)^5 10^{-9}\ \text{s} \tag{7}$$

where ν_D is the Debye frequency (~20 THz). For 5 THz longitudinal phonons with velocity of 10^4 m s^{-1} this yields a mean free path of 30 μm. However this value is not in agreement with a ν^5 extrapolation from the only experimentally measured value of τ_a by Kaplyanskii *et al.*[15,16] At a frequency of 870 GHz, the well-known 29 cm^{-1} transition in ruby, they found τ_a to be extremely anisotropic varying between 1 and 20 μs. The plane of the STJ in our present

experiment is at an inclination of approximately 60° with respect to the c-axis. We therefore expect the phonon lifetimes to be closer to the lower value, if phonons move predominantly in directions close to the normal to the surface, since these directions are far from any symmetry axis (which might cause the cancellation among third order elastic constants). Extrapolation to 5 THz yields a value for the mean free path of 1.6 μm. The origin of the discrepancy between theory and experiment is not clear. Theoretical figures are approximately an order of magnitude larger, and display less anisotropy than found in experiments.

We may also estimate the lifetime of 5 THz phonons against elastic scattering due to point defects either isotopes or impurities. We will use the expression (valid strictly for a cubic material):[17,18]

$$\tau_0(\nu) = \frac{c^3}{4\pi^3 V_0 g}\nu^{-4}, \tag{8}$$

where V_0 is the volume of the unit cell, g the coupling strength and c averaged velocity of sound. For isotope scattering $g_{\text{iso}} \simeq 1.22 \times 10^{-6}$ and for impurities at 23 ppm level $g_{\text{imp}} \simeq 1.17 \times 10^{-6}\,(\Delta M/M)^2$, where the ratio of mass difference ΔM to unit cell mass M may be taken to be around 1. Therefore, we arrive at the value of τ_D at 5 THz of 1.2×10^{-8} s and hence a mean free path of 100 μm. Thus elastic scattering is expected to be significantly weaker than anharmonic at 5 THz, and indeed across almost the whole range of acoustic phonon spectrum.

Since the propagation of 5 THz phonons across the d_1 layer is undoubtedly ballistic we may enquire as to the role and importance of phonon focussing. First we note that the focussing patterns for such high frequency phonons will be significantly altered from those given by Ref. 7 since the shape of equal energy surfaces is different from the continuum limit.[19] However, as long as d_1 is much less than the lateral dimension of the STJ, the solid angle subtended by the latter is close to 2π and no large difference can result if the anisotropic distribution of caustics is replaced by an isotropic flux. Note, that for the deeper absorption events, involving further down-conversion from 5 THz and smaller solid angles, the possibility of the STJ missing some of the caustics is undoubtedly present.

Finally we note, that the general features of the model described here also suggest a natural explanation of the charge capture ratio Q_{out}/Q_b. First, it is clear, that only phonons within a 2π solid angle at maximum can reach the STJ. In addition the transmission coefficient from the substrate into the Nb films begins to fall off rapidly beyond the angle of incidence of 60°. The solid angle for this 60° cone indeed contains 25% of the total flux (no matter whether isotropic or focused) as indicated by the base film charge capture.

The major remaining question relates to the discreteness of the direct peak, that is, why phonons around 5 THz are so much more effective in transferring energy to the STJ than those at lower frequencies. There are at least three aspects of the phonon transport which depend on frequency and hence may lead to discrimination between different phonon generations and the formation of the discrete peak. These are a) transmission across the interface with STJ, b) dependence of the collected charge on the spectrum of the entered phonons and c) dependence on phonon polarization.

Transmission across the interface has been estimated by an acoustic mismatch model.[20] However, above 2 THz the phonon spectrum in Nb deviates greatly from the continuum approximation[21] and is also very anisotropic. As a result the transmission may be greatly reduced from that estimated on the basis of the acoustic mismatch model. In addition, at higher phonon frequencies another transmission channel becomes increasingly important, which may enhance 5 THz transmission. This is due to short (atomic) scale interface irregularities, causing the diffusive scattering of incident phonons rather than coherent transmission. Scattering is governed by the phonon density for the final states and as such will take place predominantly into Nb. However, this mechanism is effective only for high frequency phonons, increasing rapidly as ν^4.[22,23]

The energy spectrum and the number of phonons among which the original x-ray energy is divided is also very important, since not all the energy of a phonon can be converted into charge. Each phonon incident on STJ can break only an integral number of Cooper pairs. The rest of its energy goes to the residual phonons with energy below $2\Delta_{\text{Nb}}$ which are lost for the detection. A single phonon of a frequency $h\nu > 2\Delta_{\text{Nb}}$ can produce in general more broken Cooper pairs than its anharmonic decay products. Thus it is important that the energies of the phonons entering the STJ should be as large as possible.

The first generation of phonons at around 5 THz which enter the Nb are mainly longitudinal,[21] while the second generation consists of predominantly transverse. Since the electron–phonon interaction is normally via deformation potential, we would expect the coupling between transverse modes and quasiparticles to be weaker.

B. The detection efficiency via the substrate

As can be seen from Fig. 5 the detection efficiency can be significantly improved if instead of the junction we use the substrate as an absorber. However, this high efficiency is limited to a small energy range, between the Al-K edge (1550 eV) and the Nb-L_{III} edge (2370 eV). It is obvious that detection efficiency depends on the material properties of the substrate. In our model d_1 relates to the mean free path for first generation phonons. Therefore, we are interested in finding an absorber with as large a ratio of d_1/L, where L is the characteristic x-ray absorption depth, as possible.

The following general requirements result from the analysis given above.

(1) For two absorber materials with equal d_1 the higher Z material is more efficient.
(2) On the other hand for two different absorber materials with the same x-ray absorption power, the less anharmonic material will result in a larger d_1.
(3) The use of the materials possessing strong elastic anisotropy which causes strong anisotropy in spontaneous an-

harmonic decay lifetimes would also be advantageous if combined with an appropriate surface orientation. In such materials a longer mean free path in the lateral direction(s) would mean that phonon energy collection for the direct peak comes from effectively larger volumes.

C. Energy resolution

The measured energy resolution is poor and needs improvement. The observed dependence of the FWHM on energy implies that the main contributions to the line shape are from spatial variations of the STJ response.

In the STJ itself, the quasiparticle tunneling probability across the STJ barrier can be significantly lower close to the edges or to the leads of the STJ, than at the center. This is due to escape through the edges or diffusion to the leads. The contribution due to spatial non-uniformities in the base film of the STJ is shown in Table I. The data were borrowed from Verhoeve *et al.*[8] They are an order of magnitude lower than the effect of spatial variations due to the phonon mediated process, also listed in the same Table I.

In the process of phonon mediated detection spatial variations of the signal arise in two ways. (i) When a photon is absorbed in the substrate, below the junction but close to its edge, the solid angle between the absorption point and STJ rapidly falls off from 2π to π at the edge and $\pi/2$ at the corner. For these direct events the phonon flux reaching the STJ diminishes rapidly. This contribution is of geometric origin and mainly controls the Gaussian FWHM. The number of x-ray absorption events near the edges of the STJ is proportional to the area of peripheral strips of width $\sim d_1$. Hence the Gaussian FWHM is governed by the parameter $4d_1/a$, where a is the side of the STJ; this ratio is about 1/5, close to the result of observations. (ii) The deviation of the experimental FWHM from the Gaussian FWHM is by definition due to absorption events taking place beyond the layer of thickness d_1. The fraction of the original x-ray energy delivered to the STJ is smaller for the reasons discussed in Sec. V A. In addition, the solid angle subtended by the STJ will be smaller, so that some of the phonon caustics may be missing from the STJ thus causing stronger spatial variations. These effects contribute to the direct peak only on the low charge side, and will be reduced in a higher Z material.

Another way to improve the resolution consists in filtering the rise time of the signal. Figure 6(a) shows a two dimensional view of the charge spectrum at 1600 eV: to each event is associated a charge output and a rise time. The number of events having the same charge output and rise time are piled up in the z-direction. The darkest regions correspond to the densest acquisition. It appears from this scatter plot that the indirect events are detected in a very large range of rise time. Selecting only the events falling in a narrow rise time window around the mean rise time for direct events, removes a non negligible amount of indirect events. Figure 6(b) shows the charge spectrum after having cut all events with rise times exceeding or smaller than the mean rise time of direct events by more than 5%. The improvement in FWHM is about 20% compared to the one measured from Fig. 1(a).

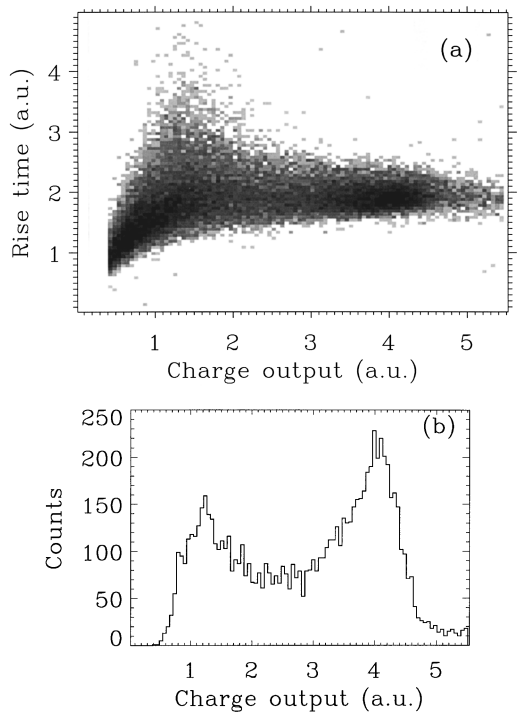

FIG. 6. (a) Scatter plot (charge output - rise time - counts) of the response of substrate events at 1600 eV for the 20×20 μm^2 device. (b) Charge spectrum corresponding to the same events, but for a restricted rise time range (mean rise time of the direct events $\pm$ 5%). This spectrum shows a FWHM for the direct events 20% lower than the FWHM in Fig. 1(a).

VI. CONCLUSIONS

Phonon mediated detection of x-rays in the range of energies from 750 to 6000 eV was studied experimentally for the Nb based STJ on crystalline sapphire substrate as an absorber. It has been clearly demonstrated that phonon mediated detection signal shows a discrete (direct) peak superimposed on a monotonic tail. The direct peak was shown to arise as a result of high (few terahertz) frequency acoustic phonon contribution originating from the x-ray absorption sites in a shallow layer below the STJ. The thickness of this layer is related to the averaged first phonon generation mean free path and does not depend on x-ray energy. Contrary to the direct peak, the phonon signal tail is due to much lower frequency acoustic phonons originating through the process of phonon down conversion. Their mean free paths are comparable to the absorber thickness. The shape of the phonon tail has been proved to be independent of the position of the absorption site and the same for both front and back illumination experimental geometry. A good quantum efficiency for the device was demonstrated, although in a limited x-ray energy range. Energy resolution is mainly affected by spatial fluctuations and proved to be relatively poor. The possibility to improve both energy resolution and quantum efficiency in the process of phonon mediated x-ray detection is analyzed, based on the results of the proposed model for the phonon transport in the detector structure.

[1] P. Verhoeve, N. Rando, P. Videler, A. Peacock, A. van Dordrecht, D. J. Goldie, J. M. Lumley, J. Howlett, M. Wallis, and R. Venn, Proc. SPIE **2283**, 172 (1994).
[2] F. Porter, D. Van Vechten, M. G. Blamire, and E. C. G. Kirk, IEEE Trans. Appl. Superconduct. **5**, 3026 (1995).
[3] C. A. Mears, S. E. Labov, and A. T. Barfknecht, Low Temp. Phys. **92**, 561 (1993).
[4] N. Rando, A. Peacock, C. Foden, A. van Dordrecht, J. M. Lumley, and C. Pereira, J. Appl. Phys. **73**, 5098 (1993).
[5] B. Neuhauser, B. Cabrera, C. J. Martoff, B. A. Young, and A. T. Lee, IEEE Trans. Nucl. Sci. **35**, 65 (1988).
[6] F. Pröbst, H. Kraus, T. Peterreins, and F. von Feilitzsch, Nucl. Instrum. Methods Phys. Res. A **280**, 251 (1989).
[7] A. G. Every, G. L. Koos, and J. P. Wolfe, Phys. Rev. B **29**, 2190 (1984).
[8] P. Verhoeve, N. Rando, J. Verveer, A. Peacock, A. van Dordrecht, P. Videler, M. Bavdaz, D. J. Goldie, T. Lederer, F. Scholze, G. Ulm, and R. Venn, Phys. Rev. B **53**, 809 (1996).
[9] N. Rando, A. Peacock, A. van Dordrecht, C. Foden, R. Engelhardt, B. G. Taylor, P. Garé, J. M. Lumley, and C. Pereira, Nucl. Instrum. Methods Phys. Res. A **313**, 173 (1992).
[10] P. Verhoeve, N. Rando, P. Videler, A. Peacock, A. van Dordrecht, R. Venn, and D. J. Goldie, in *Superconductivity and Particle Detection* (World Scientific, 1995), p. 335.
[11] S. B. Kaplan, C. C. Chi, D. Langenberg, J. J. Chang, S. Jafarey, and D. Scalapino, Phys. Rev. B **14**, 4854 (1976).
[12] D. J. Goldie, P. L. Brink, C. Patel, N. E. Booth, and G. L. Salmon, Appl. Phys. Lett. **64**, 3169 (1994).
[13] B. L. Henke, E. M. Gullikson, and J. C. Davis, Atomic Data Nucl. Data Tables **54**, No. 2 (1993).
[14] A. Berke, Solid State Commun. **61**, 313 (1987).
[15] S. A. Basun and A. A. Kaplyanskii, Sov. Phys. Solid State **22**, 2055 (1980).
[16] A. A. Kaplyanskii, S. A. Basun, and V. L. Shekhtman, J. Phys. C **6**, 439 (1981).
[17] A. G. Kozorezov, Sov. Phys. JETP **57**, 388 (1983).
[18] N. M. Guseinov and Y. B. Levinson, Zh. Éksp. Teor. Fiz. **85**, 779 (1983).
[19] H. Bialas, Z. Phys. B **27**, 121 (1977).
[20] A. Poelaert, A. Peacock, N. Rando, P. Verhoeve, and P. Videler, J. Appl. Phys. **79**, 2574 (1996).
[21] Landolt-Börnstein, New Series **III/13a**, 100 (1981).
[22] T. Nakayama, Phys. Rev. B **32**, 777 (1985).
[23] A. G. Kozorezov, T. Miyasato, and J. K. Wigmore, J. Phys: Condens. Matter **8**, 1 (1996).